Comput Mech (2005) 35: 470–480
DOI 10.1007/s00466-004-0636-3

ORIGINAL PAPER

S. Li · Y. Cheng · Y.-F. Wu

Numerical manifold method based on the method of weighted residuals

Received: 10 December 2003 / Accepted: 15 October 2004 / Published online: 17 December 2004

Abstract Usually, the governing equations of the numerical manifold method (NMM) are derived from the minimum potential energy principle. For many applied problems it is difficult to derive in general outset the functional forms of the governing equations. This obviously strongly restricts the implementation of the minimum potential energy principle or other variational principles in NMM. In fact, the governing equations of NMM can be derived from a more general method of weighted residuals. By choosing suitable weight functions, the derivation of the governing equations of the NMM from the weighted residual method leads to the same result as that derived from the minimum potential energy principle. This is demonstrated in the paper by deriving the governing equations of the NMM for linear elasticity problems, and also for Laplace's equation for which the governing equations of the NMM cannot be derived from the minimum potential energy principle. The performance of the method is illustrated by three numerical examples.

Keywords Numerical manifold method · Method of weighted residuals · Galerkin method · Manifold element · Finite covers

Y. Cheng (✉) · S. Li
Shanghai Institute of Applied Mathematics and Mechanics,
Shanghai University,
Shanghai 200072, P.R.China
Tel.: +086 021-56331043
Fax: +086-021-36033287
E-mail: ymcheng@sh163.net; shuchenli@eyou.com

Y.-F. Wu
Department of Building and Construction,
City University of Hong Kong,
Hong Kong
Tel: 852-27844259
Fax: 852-27887612
E-mail: yfwu00@cityu.edu.hk

1 Introduction

The numerical manifold method (NMM) (Shi, 1992, 1996 and 1997) is a newly developed computational approach for blocky systems that is applicable to general continuous and dis-continuous media. The method is derived from the finite cover approximation theory and gains her name after the mathematical notion of manifold. It demonstrates a good consistency with both the conventional finite element method (FEM) and the discontinuous deformation analysis (DDA) (Shi, 1988). Because of this discrete element root and the unified mathematical framework, the manifold method can be used both in integrating the continuum and in discrete analysis .Due to its unique mathematical features as detailed in the next section, the manifold method is more suitable than other numerical methods for problems with discontinuous and moving boundaries such a crack development and free surface flow.

Usually, the governing equations of the numerical manifold method are derived from the minimum potential energy principle (Shi, 1996). For many applied problems, e.g. heat conduction and potential flow, it is very difficult to derive in general outset the functional forms of the governing equations. This obviously strongly restricts the implementation of the minimum potential energy principle or other variational principles in NMM. In fact, the governing equations of the NMM can be derived from a more general method of weighted residual (MWR).

The MWR is a numerical method for solving partial differential equations (Xu, 1987). At the same time, the method unifies the mathematical foundation of many numerical methods, such as finite element method (Zienkiewicz, 1977), boundary element method (Ji, 1997; Cheng, 1996) and element-free Galerkin method (Belytschko, 1994). Due to its nature of generality the MWR enriches the mathematical foundation of the numerical methods and extends their fields of application.

In the paper, the governing equations of the numerical manifold are derived by the method of weighted residuals. The derivation leads to the same result as that derived from the minimum potential energy principle by choosing suitable weight functions. This is demonstrated by the derivation of the governing equations of the NMM for two typical cases in the paper: 1) linear elasticity problem; and 2) the Laplace's equation for which the NMM cannot be derived from the minimum potential energy principle. The method developed in this paper is more general than that of the minimum potential energy principle. The work developed in this paper enriches the mathematical foundation of the NMM and extends its field of application.

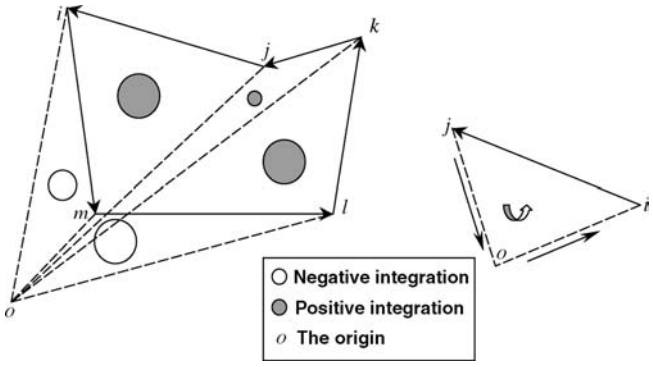

Fig. 2 Orientation of a triangle *oij* in the integration

2 The theory of numerical manifold method

The basic structure of the NMM (Shi, 1997 and Ku, 2001) is shown in Fig. 1, which shows that NMM consists of three main parts: block kinematics, finite covering systems, and the simplex integration method.

NMM inherits the block kinematics and contact-detection techniques from DDA method. The contact detection has two constrains: no penetration and no tension between blocks, which are described by inequalities. Using block kinematics, NMM can deal with the mechanical response of a block system under general loading and moving boundary conditions when body movement and large deformation occur simultaneously.

In NMM, numerical integration such as Gauss integration method is not needed. Mapping to convert an arbitrary shape into a regular pattern is not required. Therefore, the physical boundary of a manifold element can take any shape. The NMM uses the simplex integration method, in which an arbitrary domain of integration of a function is converted into many triangles in which the integration can be calculated analytically to ensure high precision (see Fig. 2).

The finite cover system is one of the most innovative features of the manifold method. Details of the system are described in the following section.

2.1 The finite cover systems

The finite cover systems are made up of the mathematical meshes and the physical meshes in the NMM. The physical mesh is a unique portrait of the physical domain of a problem. It defines the integration fields. The physical mesh includes the boundary of the material volume, joints, blocks and the interfaces of different materials zones. It represents material condition that cannot be chosen arbitrarily. The mathematical mesh defines the fine or rough approximation of unknown functions. It can be a mesh of some regular pattern, or a combination of some arbitrary figures. This mesh is chosen according to the problem geometry, solution accuracy requirements, and the physical property zoning. The mathematical mesh is used for building mathematical covers that present small regions of the whole field and can be any shape and sizes. They can overlap each other and need not coincide with the physical mesh. However, the whole mesh has to be large enough to cover every point of the physical mesh. Overlapping these two meshes provides a manifold description. The intersection of the mathematical cover and the physical mesh, or the common region of the two systems, defines the region of physical covers. A common area of the overlapped physical covers corresponds to an element in the manifold method. Piecing together all the common areas produces a complete cover of the whole field without overlapping. The mathematical mesh and the physical mesh are generally independent. The mathematical covers reflect the physical mesh through the application of weight functions. It is worth mentioning that the covers of the manifold method can span discontinuity boundaries. In addition, the manifold method does not require a mathematical mesh to conform to the physical boundary of a problem, and the mathematical cover can be partially out of the material volume. Therefore, the same size and shape to all the covers can always be used for the complicated geometric shapes of the material volumes and joint distributions. Further details of the geometrical aspect of manifolds can be found in the works by Shi (1997) and Terada (2003).

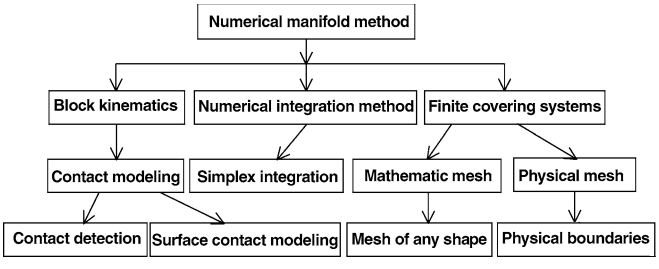

Fig. 1 Basic structure of the numerical manifold method

The above concept of cover systems is illustrated in the example shown in Fig. 3. The circle and the hexagon mesh are arbitrarily selected as the mathematical mesh, as shown in Fig. 3a. Fig. 3b shows the structure containing a crack that defines the physical mesh. The

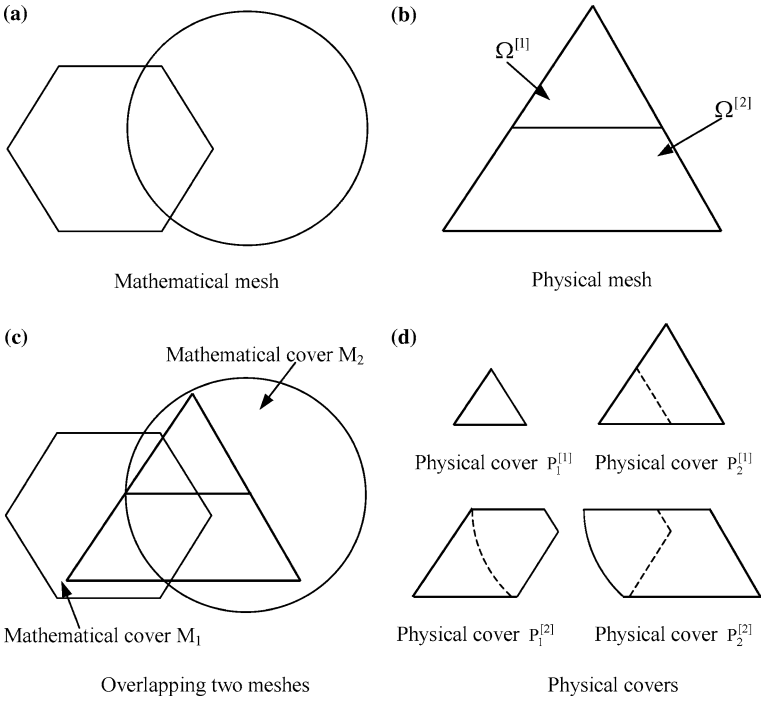

Fig. 3 Mathematical and physical covers

common region of the mathematical cover M_I and the physical mesh $\Omega^{[\alpha]}$ forms the physical covers, and is denoted by $P_I^{[\alpha]}$ in Fig. 3. These two meshes provide a covered manifold of the problem.

Based on the concept of covering systems, the approximation method by means of finite covers can be formulated that is described in the next section.

2.2 Covers and weight functions

Theoretically any shape of covers can be used in NMM. However integration of manifold elements is related to the cover shape, a reasonable choice of cover shape is very important (Chen, 1998). It is very convenient to use triangular meshes as shown in Fig. 4, where each intersection point of the meshes is the center point of a cover and is called a star. All the triangles around the star form a hexagonal cover. A triangle is exactly the common area of three hexagonal covers as shown in Fig. 4. The stars in the three hexagonal covers form the three vertices of a triangle. The triangle is called a manifold element.

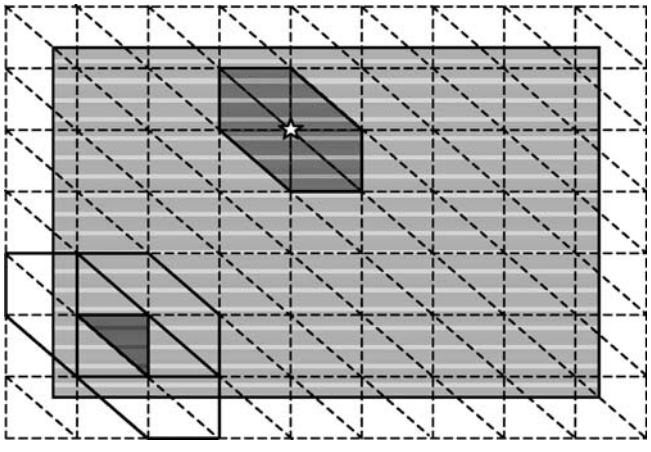

Fig. 4 Covers and manifold element formed from triangular meshes

The schematic configuration of the weight function for a hexagonal cover is shown in Fig. 5. The weight function equals to 1 at the center point and declines linearly to 0 at all the sides of the cover as shown in Fig. 5a. The weight function is a piecewise function of six linear functions corresponding to six triangles of the cover, see Fig. 5b. The weight function $w_i(x,y)$ is the partition of unity function that satisfies

$$w_i(x,y) \geq 0 \qquad (x,y) \in C_i \tag{1}$$

$$w_i(x,y) = 0 \qquad (x,y) \notin C_i \tag{2}$$

$$\sum_{i=1}^{m} w_i(x,y) = 1 \qquad (x,y) \in E \tag{3}$$

where C_i is a cover; E is a manifold element; and m is the number of covers that form the manifold element.

Suppose that three covers i, j and k form a manifold element E, the three weight functions of the three covers are

$$\begin{Bmatrix} w_{e(1)}(x,y) \\ w_{e(2)}(x,y) \\ w_{e(3)}(x,y) \end{Bmatrix} = \begin{Bmatrix} f_{11} + f_{12}x + f_{13}y \\ f_{21} + f_{22}x + f_{23}y \\ f_{31} + f_{32}x + f_{33}y \end{Bmatrix} = \begin{bmatrix} f_{11} & f_{12} & f_{13} \\ f_{21} & f_{22} & f_{23} \\ f_{31} & f_{32} & f_{33} \end{bmatrix} \begin{Bmatrix} 1 \\ x \\ y \end{Bmatrix} \tag{4}$$

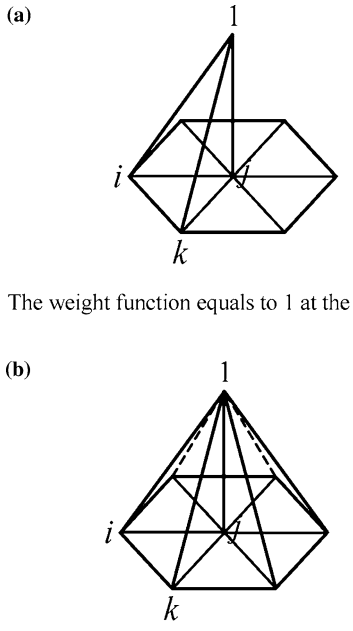

Fig. 5 The weight functions defined in a hexagonal cover

where

$$\begin{bmatrix} f_{11} & f_{12} & f_{13} \\ f_{21} & f_{22} & f_{23} \\ f_{31} & f_{32} & f_{33} \end{bmatrix}^T = \frac{1}{\Delta} \begin{bmatrix} x_{e(j)}y_{e(k)} - x_{e(k)}y_{e(j)} & x_{e(k)}y_{e(i)} - x_{e(i)}y_{e(k)} & x_{e(i)}y_{e(j)} - x_{e(j)}y_{e(i)} \\ y_{e(j)} - y_{e(k)} & y_{e(k)} - y_{e(i)} & y_{e(i)} - y_{e(j)} \\ x_{e(k)} - x_{e(j)} & x_{e(i)} - x_{e(k)} & x_{e(j)} - x_{e(i)} \end{bmatrix} \tag{5}$$

and

$$\Delta = \begin{vmatrix} 1 & x_{e(i)} & y_{e(i)} \\ 1 & x_{e(j)} & y_{e(j)} \\ 1 & x_{e(k)} & y_{e(k)} \end{vmatrix} \tag{6}$$

2.3 The approximation functions

Supposing that m overlapped covers $(C_i, i = 1, \ldots, m)$ form a manifold element E, the test functions $u(x, y)$ can be obtained by taking the weighted average of the m cover functions u_i,

$$u(x,y) = \sum_{i=1}^{m} w_i(x,y)u_i(x,y), \quad (x,y) \in E \tag{7}$$

Since the whole field is completely covered by the manifold elements without overlapping, the overall approximation functions can be expressed by joining the piecewise functions $u(x, y)$ defined in each element.

According to Eq. (7), for a two-dimensional displacement field problem, the displacement functions in an element E can be written as

$$u(x,y) = w_i(x,y)u_i(x,y) + w_j(x,y)u_j(x,y) + w_k(x,y)u_k(x,y) \tag{8a}$$

$$v(x,y) = w_i(x,y)v_i(x,y) + w_j(x,y)v_j(x,y) + w_k(x,y)v_k(x,y) \tag{8b}$$

where $u_l(x,y), v_l(x,y), l = i, j, k$ are cover displacement functions; $w_l(x,y), l = i, j, k$ are weight functions given by Eq. (4).

The cover displacement functions can also be expressed as

$$u_l(x,y) = \boldsymbol{P}_l(x,y)\boldsymbol{U}_l \tag{9}$$

$$v_l(x,y) = \boldsymbol{P}_l(x,y)\boldsymbol{V}_l \tag{10}$$

where $\boldsymbol{P}_l(x,y), l = i, j, k$ are the basis functions,

$$\boldsymbol{P}_l(x,y) = 1 \quad \text{(Constant basis functions)} \tag{11a}$$

$$\mathbf{P}_l(x,y) = (1,x,y) \quad \text{(Linear basis functions)} \tag{11b}$$

$$\mathbf{P}_l(x,y) = (1,x,y,x^2,xy,y^2) \quad \text{(Quadratic basis functions)} \tag{11c}$$

$\mathbf{U}_l$ and $\mathbf{V}_l$ are unknown coefficients of the basis functions.

Considering Eq. (4, 8–11a), the cover displacement function from constant basis generates the linear displacement function of the manifold element.

$$\begin{bmatrix} u(x,y) \\ v(x,y) \end{bmatrix} = \begin{bmatrix} w_i(x,y) & 0 & w_j(x,y) & 0 & w_k(x,y) & 0 \\ 0 & w_i(x,y) & 0 & w_j(x,y) & 0 & w_k(x,y) \end{bmatrix} \begin{bmatrix} u_i \\ v_i \\ u_j \\ v_j \\ u_k \\ v_k \end{bmatrix} \tag{12a}$$

$$\begin{bmatrix} u(x,y) \\ v(x,y) \end{bmatrix} = [\, \boldsymbol{T}_i(x,y) \quad \boldsymbol{T}_j(x,y) \quad \boldsymbol{T}_k(x,y) \,] \begin{bmatrix} \boldsymbol{D}_i \\ \boldsymbol{D}_j \\ \boldsymbol{D}_k \end{bmatrix} \tag{12b}$$

$$= \boldsymbol{T}_e(x,y)\boldsymbol{D}_e$$

where

$$\boldsymbol{T}_l(x,y) = \begin{bmatrix} w_l(x,y) & 0 \\ 0 & w_l(x,y) \end{bmatrix} \tag{13}$$

$$\boldsymbol{D}_l = \begin{bmatrix} u_l \\ v_l \end{bmatrix}, \quad l = i,j,k \tag{14}$$

3 The numerical manifold method based on the method of weighted residual

The governing equations and the boundary conditions of linear elasticity are

$$\sigma_{ij,j} + f_i = 0 \quad \text{in } \Omega \tag{15}$$

$$\sigma_{ij} n_j = \bar{T}_i \quad \text{on } S_\sigma \tag{16}$$

$$u_i = \bar{u}_i \quad \text{on } S_u \tag{17}$$

where Ω is a solving domain; $\bar{u}_i$ is given displacements on the boundary S_u; $\bar{T}_i$ is given tractions on the boundary S_σ; and $S_u \cup S_\sigma = S$, n_j is the outward normal to the boundary of Ω

The strain-displacement relationship can be expressed in a matrix form as

$$\varepsilon = \boldsymbol{L}\boldsymbol{u}^h = (\boldsymbol{L}\boldsymbol{T}_e)\boldsymbol{D}_e = \boldsymbol{B}_e\boldsymbol{D}_e \tag{18}$$

where $\boldsymbol{L}$ is a differential operator matrix, and for two-dimensional problems

$$\boldsymbol{L} = \begin{bmatrix} \frac{\partial}{\partial x} & 0 & \frac{\partial}{\partial y} \\ 0 & \frac{\partial}{\partial y} & \frac{\partial}{\partial x} \end{bmatrix}^T \tag{19}$$

$$\boldsymbol{B}_e = \boldsymbol{L}(\boldsymbol{T}_e) \tag{20}$$

The stress can be expressed as

$$\sigma = \boldsymbol{E}\varepsilon = \boldsymbol{E}\boldsymbol{B}_e\boldsymbol{D}_e \tag{21}$$

where $\boldsymbol{E}$ is the elastic constant matrix.

Using the method of weighted residuals we have

$$\int_\Omega W_i R_i d\Omega = 0 \tag{22}$$

where W_i is the weight function; and R_i is the residual.

Substituting the approximation functions Eq. (12b) into the governing equation, we obtain

$$\sigma_{ij,j} + f_i = R_i \tag{23}$$

Substituting Eq. (23) into Eq. (22), we have

$$\int_\Omega W_i(\sigma_{ij,j} + f_i) d\Omega = 0 \tag{24}$$

Integrating by parts Eq. (24) can be expressed as the following form

$$\int_s W_i \sigma_{ij} n_j dS - \int_\Omega W_{i,j}\sigma_{ij} d\Omega + \int_\Omega W_i f_i d\Omega = 0 \tag{25}$$

Appling the boundary condition Eq. (16), Eq. (25) gives

$$\int_{S_\sigma} W_i \bar{T}_i dS_\sigma - \int_\Omega W_{i,j}\sigma_{ij} d\Omega + \int_\Omega W_i f_i d\Omega = 0 \tag{26}$$

or

$$\int_\Omega W_{i,j}\sigma_{ij} d\Omega = \int_{S_\sigma} W_i \bar{T}_i dS_\sigma + \int_\Omega W_i f_i d\Omega \tag{27}$$

Let the weight functions W_i equal to the shape functions T_{ij} in the approximation functions u_i^h, Eq. (27) is the classical Galerkin formula. Eq. (27) can be rewritten as

$$\int_\Omega T_{ij,j}\sigma_{ij} d\Omega = \int_{S_\sigma} T_{ij}\bar{T}_i dS_\sigma + \int_\Omega T_{ij} f_i d\Omega \tag{28}$$

The above expressions can be expressed in a matrix form, i.e.

$$\int_\Omega (\boldsymbol{L}\boldsymbol{T}_e)^T \sigma d\Omega = \int_{S_\sigma} (\boldsymbol{T}_e)^T \boldsymbol{T} dS_\sigma + \int_\Omega (\boldsymbol{T}_e)^T \boldsymbol{f} d\Omega \tag{29}$$

Substituting Eq. (18) and Eq. (21) into Eq. (29), we obtain

$$\sum_e \int_{\Omega_e} \boldsymbol{B}_e^T \boldsymbol{E}\boldsymbol{B}_e\boldsymbol{D}_e d\Omega_e = \sum_e \int_{S_{\sigma e}} \boldsymbol{T}_e^T \boldsymbol{T} ds_{\sigma e} + \sum_e \int_{\Omega_e} \boldsymbol{T}_e^T \boldsymbol{f} d\Omega_e \tag{30}$$

Eq. (30) can be rewritten as

$$\sum_e \int_{\Omega_e} \boldsymbol{B}_e^T \boldsymbol{E}\boldsymbol{B}_e d\Omega_e \boldsymbol{D}_e = \sum_e \int_{S_{\sigma e}} \boldsymbol{T}_e^T \boldsymbol{T} dS_{\sigma e} + \sum_e \int_{\Omega_e} \boldsymbol{T}_e^T \boldsymbol{f} d\Omega_e \tag{31}$$

Let

$$\int_{\Omega_e} \boldsymbol{B}_e^T \boldsymbol{E}\boldsymbol{B}_e d\Omega_e = \boldsymbol{K}_e \tag{32}$$

$$\int_{S_{\sigma e}} \mathbf{T}_e^T \mathbf{T} dS_{se} = \mathbf{F}_e^s \tag{33}$$

$$\int_{\Omega_e} \mathbf{T}_e^T \mathbf{f} d\Omega_e = f F_e^b \tag{34}$$

$$\mathbf{F}_e = \mathbf{F}_e^s + \mathbf{F}_e^b \tag{35}$$

where $\boldsymbol{K}_e$ is called the element stiffness matrix of manifold element, $\boldsymbol{F}_e$ is called the loading matrix.

Eq. (31) can be rewritten as

$$\boldsymbol{K}\boldsymbol{D} = \boldsymbol{F} \tag{39}$$

where $\boldsymbol{D}$ is the coefficient matrix.

The above expressions can be written in explicit form, i.e.

$$\begin{pmatrix} K_{11} & K_{12} & K_{13} & \cdots & K_{1n} \\ K_{21} & K_{22} & K_{23} & \cdots & K_{2n} \\ K_{31} & K_{32} & K_{33} & \cdots & K_{3n} \\ \vdots & \vdots & \vdots & \ddots & \vdots \\ K_{n1} & K_{n2} & K_{n3} & \cdots & K_{nn} \end{pmatrix} \begin{Bmatrix} D_1 \\ D_2 \\ D_3 \\ \vdots \\ D_n \end{Bmatrix} = \begin{Bmatrix} F_1 \\ F_2 \\ F_3 \\ \vdots \\ F_n \end{Bmatrix} \tag{40}$$

From the above process, we can see that the derivation of the governing equations of the NMM from the weighted residual method leads to the same result as that derived from the minimum potential energy principle by choosing suitable weight functions.

Using Eqs. (4), (13) and (20), $\boldsymbol{B}_e$ is obtained as

$$\boldsymbol{B}_{e(i)} = \begin{pmatrix} f_{i2} & 0 & f_{i3} \\ 0 & f_{i3} & f_{i2} \end{pmatrix}^T \tag{41}$$

Substituting Eq. (41) into Eq. (32), we obtain

$$\begin{aligned} \boldsymbol{K}_{e(r)e(s)} &= A^e \boldsymbol{B}_{e(r)}^T \boldsymbol{E} \boldsymbol{B}_{e(s)} \\ &= A^e \begin{bmatrix} \boldsymbol{B}_{e(i)}^T \\ \boldsymbol{B}_{e(j)}^T \\ \boldsymbol{B}_{e(k)}^T \end{bmatrix} [\boldsymbol{E}] \begin{bmatrix} \boldsymbol{B}_{e(i)} & \boldsymbol{B}_{e(j)} & \boldsymbol{B}_{e(k)} \end{bmatrix} \end{aligned} \tag{42}$$

where A^e is the area of manifold element e that can be obtained by simplex integration.

Substituting Eq. (13) into Eq. (33), we obtain

$$\int_{S_{\sigma e}} \boldsymbol{T}_e^T \boldsymbol{T} dS_{se} = \int_{S_{\sigma e}} [\boldsymbol{T}_{e(r)}(x,y)]^T dS \begin{bmatrix} \bar{T}_x \\ \bar{T}_y \end{bmatrix}$$

$$= \begin{bmatrix} f_{i1}S^e + f_{i2}S_x^e + f_{i3}S_y^e & 0 \\ 0 & f_{i1}S^e + f_{i2}S_x^e + f_{i3}S_y^e \end{bmatrix} \begin{bmatrix} \bar{T}_x \\ \bar{T}_y \end{bmatrix} \tag{43}$$

where S^e, S_x^e, and S_y^e are obtained by integration on the boundary, i.e.

$$S^e = \int_S dS \tag{44}$$

$$S_x^e = \int_S x dS \tag{45}$$

$$S_y^e = \int_S y dS \tag{46}$$

For a point load vector, if it is applied at coordinate(x_0, y_0), Eq. (43) can be rewritten as

$$\boldsymbol{T}_e^T \boldsymbol{T} = [\boldsymbol{T}_{e(r)}(x_0, y_0)]^T \begin{bmatrix} F_x \\ F_y \end{bmatrix} = \boldsymbol{F}_{e(r)} \tag{47}$$

For body forces, Eq. (34) can be rewritten as

$$\int_{\Omega_e} \boldsymbol{T}_e^T \boldsymbol{f} d\Omega_e = \int_{\Omega_e} [\boldsymbol{T}_e(x,y)]^T d\Omega_e \begin{bmatrix} f_x \\ f_y \end{bmatrix} = \boldsymbol{F}_e^b \tag{48}$$

where the integration can be given as

$$\int\int_{\Omega} [\boldsymbol{T}_{e(i)}]^T dxdy = \int\int_{\Omega} \begin{bmatrix} w_{e(i)}(x,y) & 0 \\ 0 & w_{e(i)}(x,y) \end{bmatrix} dxdy$$

$$= \begin{bmatrix} f_{i1}A^e + f_{i2}A_x^e + f_{i3}A_y^e & 0 \\ 0 & f_{i1}A^e + f_{i2}A_x^e + f_{i3}A_y^e \end{bmatrix} \tag{49}$$

and A^e, A_x^e and A_y^e can be obtained by simplex integrations.

The above procedure leads to the global stiffness matrix and the loading matrix. These matrixes have the same expression as that obtained from the minimum potential energy principle.

4 Numerical manifold method of the laplace equation

Laplace's equation is the governing equation for a wide range of physical phenomena. e.g. heat conduction and potential flow. In this section the NMM formulation of the Laplace's equation is developed. Laplace's equation is given by

$$\frac{\partial^2 u}{\partial x^2} + \frac{\partial^2 u}{\partial y^2} = 0 \quad \text{in } \Omega \tag{50}$$

For a two-dimensional domain Ω, the boundary conditions are

$$\frac{\partial u}{\partial n} = \bar{q} \quad \text{on } S_1 \tag{51}$$

and

$$u = \bar{u} \quad \text{on } S_2 \tag{52}$$

where the boundary conditions $\bar{u}$ and $\bar{q}$ define the boundary value and flux, respectively; n is the outward normal unit vector at the boundary; and S_1 and S_2 are boundaries for essential and natural boundary conditions, respectively. For the well-posed boundary value problem,

$$S_1 \cup S_2 = S \tag{53}$$

and

$$S_1 \cap S_2 = \phi \tag{54}$$

in which $\cup$ and $\cap$ denote sum and intersection respectively, and S is the total boundary of the domain Ω.

Integration of weighted residual of the differential equation is given by

$$I = \int_{\Omega} w \left(\frac{\partial^2 u}{\partial x^2} + \frac{\partial^2 u}{\partial y^2} \right) d\Omega = 0 \tag{55}$$

Integrating Eq. (55) by parts and applying boundary condition Eq. (51) give

$$\begin{aligned} I &= \int_{\Omega} \left[\frac{\partial^2 u}{\partial x^2} + \frac{\partial^2 u}{\partial y^2} \right] \boldsymbol{T} d\Omega \\ &= \int_{S_1} \frac{\partial u}{\partial x} \boldsymbol{T} n_x dS + \int_{S_1} \frac{\partial u}{\partial y} \boldsymbol{T} n_y dS - \int_{\Omega} \left(\frac{\partial u}{\partial x} \frac{\partial \boldsymbol{T}}{\partial x} + \frac{\partial u}{\partial y} \frac{\partial \boldsymbol{T}}{\partial y} \right) d\Omega \\ &= \int_{S_1} \left(\frac{\partial u}{\partial x} n_x + \frac{\partial u}{\partial y} n_y \right) \boldsymbol{T} dS - \int_{\Omega} \left(\frac{\partial u}{\partial x} \frac{\partial \boldsymbol{T}}{\partial x} + \frac{\partial u}{tialy} \frac{\partial \boldsymbol{T}}{\partial y} \right) d\Omega \\ &= \int_{S_1} \bar{q} \boldsymbol{T} dS - \int_{\Omega} \left(\frac{\partial u}{\partial x} \frac{\partial \boldsymbol{T}}{\partial x} + \frac{\partial u}{\partial y} \frac{\partial \boldsymbol{T}}{\partial y} \right) d\Omega \end{aligned} \tag{56}$$

Substituting Eqs. (13) and (56) into Eq. (55) gives

$$\sum_e \left[\int_{S_1} \bar{q} \boldsymbol{T}_{e(i)} dS - \int_{\Omega_e} \left(\frac{\partial \boldsymbol{T}_{e(i)}}{\partial x} \frac{\partial \boldsymbol{T}_{e(j)}}{\partial x} + \frac{\partial \boldsymbol{T}_{e(i)}}{\partial y} \frac{\partial \boldsymbol{T}_{e(j)}}{\partial y} \right) \boldsymbol{D}_e d\Omega_e \right] = 0 \tag{57}$$

Let

$$\int_{S_1} \bar{q} \boldsymbol{T}_{e(i)} dS = \boldsymbol{F}_{e(i)} \tag{58}$$

$$\int_{\Omega_e} \left(\frac{\partial \boldsymbol{T}_{e(i)}}{\partial x} \frac{\partial \boldsymbol{T}_{e(j)}}{\partial x} + \frac{\partial \boldsymbol{T}_{e(i)}}{\partial y} \frac{\partial \boldsymbol{T}_{e(j)}}{\partial y} \right) d\Omega_e = \boldsymbol{K}_{e(i)e(j)} \tag{59}$$

The following governing equations is obtained

$$\boldsymbol{KD} = \boldsymbol{F} \tag{60}$$

Substituting Eqs. (4) and (13) into Eq. (59), the element stiffness matrix is written as

$$K_{e(i)e(j)} = \int_{\Omega_e} \left(\frac{\partial i T_{e(i)}}{\partial x} \frac{\partial \boldsymbol{T}_{e(j)}}{\partial x} + \frac{\partial \boldsymbol{T}_{e(i)}}{\partial y} \frac{\partial \boldsymbol{T}_{e(j)}}{\partial y} \right) d\Omega_e$$

$$= A^e \begin{bmatrix} f_{ij} f_{jj} + f_{ik} f_{jk} & 0 \\ 0 & f_{ij} f_{jj} + f_{ik} f_{jk} \end{bmatrix}, (i, j, k = 1, 2, 3) \tag{61}$$

Substituting Eq. (13) into Eq. (58) gives

$$\boldsymbol{F}_{e(i)} = \int_{S_1} \bar{q} \boldsymbol{T}_{e(i)} dS = \bar{q} \int_{S_1} \boldsymbol{T}_{e(i)} dS$$

$$= \begin{bmatrix} f_{ii} S^e + f_{ij} S^e_x + f_{ik} S^e_y & 0 \\ 0 & f_{ii} S^e + f_{ij} S^e_x + f_{ik} S^e_y \end{bmatrix} \begin{bmatrix} \bar{q}_x \\ \bar{q}_y \end{bmatrix} \tag{62}$$

where S^e, S^e_x, and S^e_y are obtained by integration on the boundary.

5 Simplex integration

Direct integration over each simplex in the chain is suggested (Shi, 1992), because many functions, in particular polynomials, can be integrated analytically on a simplex. With a coordinate transformation, analytical results can be obtained for integration over an arbitrary n-dimensional Euclidean space. This scheme is explained with an R^2 example. A physical domain (i, j, k, l, m) and a triangulation are shown in Fig. 2. For both, the oriented boundaries are consisted of the same sequence ordered edges: $(i, m) + (m, l) + (l, k) + (k, j) + (j, i)$. A boundary preserved triangulation can easily be achieved by connecting each pair to one single point. The coordinate origin, $o(0, 0)$, is a desirable choice in which a two-chain obtained equals $(o, i, m) + (o, m, l) + (o, l, k) + (o, k, j) + (0, j, i)$. Each set of the three ordered vertices is a two-simplex (Lin, 2003).

With a simplex chain representation of a manifold element E, the integration becomes a sum of simplex integration as follows

$$A^e = \int_{\Omega_e} dK = \int_E dK = \sum_i \int_{S_{Ei}} dK_i \tag{63}$$

Each of the integration on a simplex can be evaluated analytically. This is carried out in two steps. First, an integration in terms of area coordinates, L_1, L_2 and L_3, over a coordinate simplex, i.e., simplex with vertices $U_0(0, 0)$, $U_1(1, 0)$, $U_2(0, 1)$, can be evaluated analytically. Namely,

$$\int \int_{U_0 U_1 U2} L_0^{n_0} L_1^{n_1} L_2^{n_2} dL_1 dL_2 = \frac{n_0! n_1! n_2!}{(n_0 + n_1 + n_2 + 2)!} \tag{64}$$

Second, a general integration in terms of x and y over a simplex with vertices $o(x_0, y_0)$, $i(x_1, y_1)$ and $j(x_2, y_2)$ is evaluated by the coordinate transformation

$$\begin{cases} x = x_0 L_0 + x_1 L_1 + x_2 L_2 \\ y = y_0 L_0 + y_1 L_1 + y_2 L_2 \\ 1 = L_0 + L_1 + L_2 \end{cases} \tag{65}$$

such that

$$\int \int_{oij} x^a y^b dx dy = \text{sign}(J) \int \int (x_0 L_0 + x_1 L_1 + x_2 L_2)^a \times (y_0 L_0 + y_1 L_1 + y_2 L_2)^b dL_1 dL_2 \tag{66}$$

where, sign(J) is a signed Jacobian.

Taking the case of $a = 2$ and $b = 3$, for example, and by choosing $x_0 = 0, y_0 = 0$, an integration over an element domain containing n vertices becomes

$$\begin{aligned} \int \int_{\Omega_e} x^2 y^3 dx dy = \sum_{k=1}^{n} J_k \cdot \Bigg[& \frac{5!}{8!} (x_k^2 y_k^3 + x_{k+1}^2 y_{k+1}^3) \\ & + \frac{4!}{7!} (3 x_k^2 y_k^2 y_{k+1} + 3 x_{k+1}^2 y_k y_{k+1}^2 \\ & + 2 x_k x_{k+1} y_{k+1}^3 + 2 x_k x_{k+1} y_k^3) \Bigg] \\ & + \frac{2!3!}{7!} (x_k^2 y_{k+1}^3 + x_{k+1}^2 y_k^3 + 3 x_k^2 y_{k+1}^2 y_k \\ & + 3 x_{k+1}^2 y_{k+1} y_k^2 + 6 x_k x_{k+1} y_k^2 y_{k+1} \\ & + 6 x_k x_{k+1} y_k y_{k+1}^2) \end{aligned} \tag{67}$$

where $J_k = (x_k y_{k+1} - y_k x_{k+1})/2$; x_k, y_k are the coordinates of the kth vertex, and $n + 1$ vertex is a repeat of the first vertex.

6 Illustrative examples

6.1 Beam bending under point load at mid-span

In Fig. 6 a beam of 10 m long and 1 m high is loaded with a point load of $P = 200$ N at the mid-span. The beam is simply supported with a pinned support at the

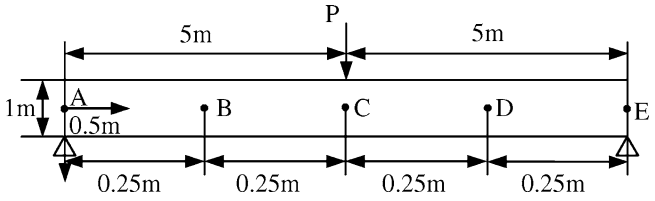

Fig. 6 Beam bending problem

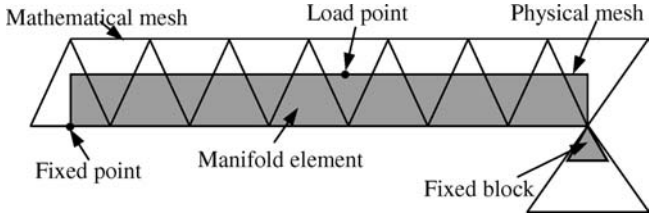

Fig. 7 The model of beam bending for the manifold method

left hand side and a roller support at the right hand side. The Young's modulus and Poisson's ratio of the beam are $E = 1.0 \times 10^5$ N/m^2 and $\upsilon = 0.24$, respectively. The points indicated by A, B, C, D, and E are reference points for comparing the numerical results with the analytical solution.

The model for the NMM calculation is shown in Fig. 7, in which the left bottom end point is fixed and the right end is laid on another fixed block so as to allow for the horizontal deformation of the beam on the support. Triangular meshes are used and a total of 15 elements are formed in Fig. 8.The stiffness of the spring for both normal and shear directions is 1.0×10^7 N/m. The maximum allowed displacement ratio in a step is 0.01 per cent. Two and half thousand steps with time interval $\Delta t = 0.01$s have been calculated for the whole deformation.

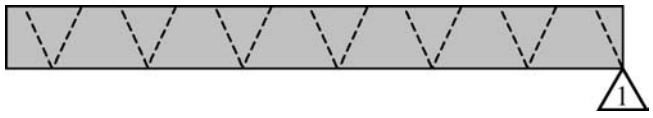

Fig. 8 Manifold element of the beam

The analytical solution of the vertical displacement of the problem is given by (Chen, 1998).

$$v(x) = -\frac{P}{12EI}x^3 + \frac{Pl^2}{16EI}x \quad (0 \le x \le \frac{1}{2}) \tag{68}$$

where I is the moment of inertia and l is the length of the beam.

The analytical and numerical results of the vertical displacements at the reference points are calculated and listed in Table 1. Fifteen and 100 elements are used in the numerical solution for comparison. It can be seen from the table that the numerical results with 100 manifold elements agree well with the analytical results. The results with the 15 elements are not satisfactory.

6.2. Tensile edge crack

A rectangular plate with an edge crack is shown in Fig. 9. The plate is loaded in tension at the top with

Table 1 The vertical displacements of the reference points

The reference points	Analytical Solutions (m)	The results from NMM (m)	
		(15 elements)	(100 elements)
A (x = 0.00 m)	0.000	0.000	0.000
B (x = 2.50 m)	0.344	0.055	0.342
C (x = 5.00 m)	0.500	0.086	0.496
D (x = 7.50 m)	0.344	0.054	0.339
E (x = 10.0 m)	0.000	0.000	0.000

Fig. 9 Edge crack problem

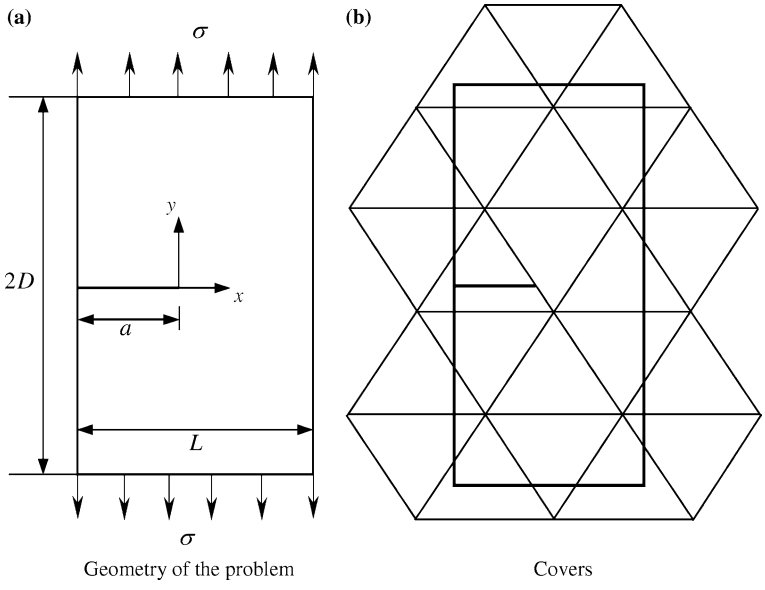

$\sigma = 0.2$ Gpa and essential boundary conditions are applied to the bottom of the plate. The following parameters are used in the example: $L = 52$ mm, $D = 20$ mm, $a = 12$ mm; Elastic modulus $E = 76$ Gpa, Poisson's ratio$\mu = 0.286$, and plane strain state of deformation is assumed.

The mode I stress intensity factors corrected for finite geometry is given by

$$K_I = C\sigma\sqrt{a\pi} \tag{69}$$

where the correction is given by Ewalds and Wanhill (Ewalds, 1989) as

$$C = 1.12 - 0.231(a/L) + 10.55(a/L)^2 - 21.72(a/L)^3 + 30.39(a/L)^4 \tag{70}$$

The analytical stress intensity factor K_I normalized by $\sigma\sqrt{a\pi}$ is calculated to be $C = 1.34$.

The manifold elements used in the numerical calculation are shown in Fig. 10. The numerical result of the normalized stress intensity factor is calculated to be C = 1.36. It agrees with the analytical solution very well. Fig. 11 and Fig. 12 show the comparison between the analytical and numerical results of the singular stress field near the crack tip. The y-displacement distributions are shown in Fig. 13. From Figs. 11, 12 and 13, we can see that the numerical solutions agree with the analytical solution very well at the crack tip.

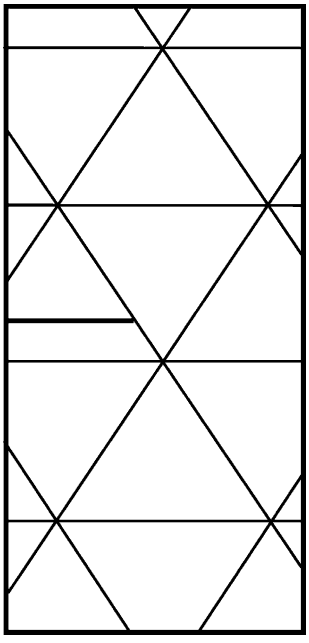

Fig. 10 Manifold elements of the edge crack problem

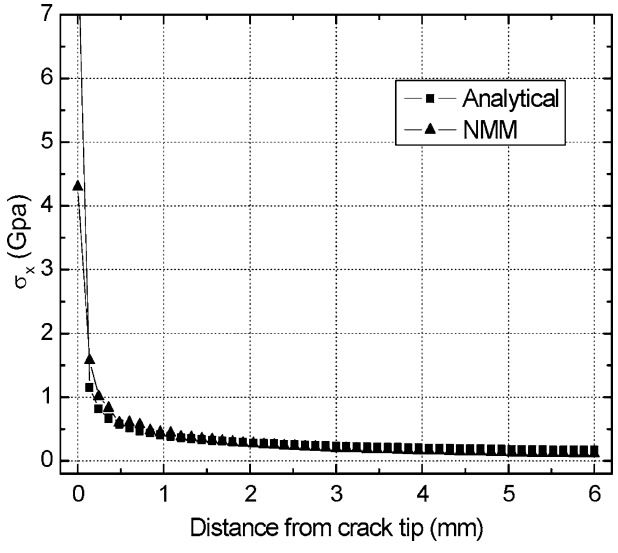

Fig. 11 Stresses σ_x ahead of the crack tip for the edge crack problem

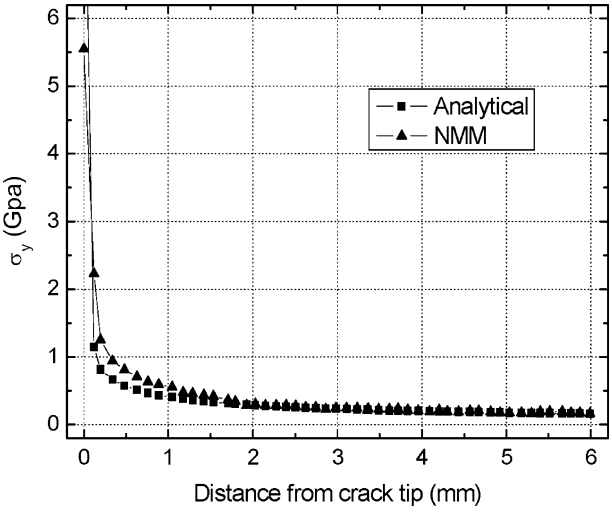

Fig. 12 Stresses σ_y ahead of the crack tip for the edge crack problem

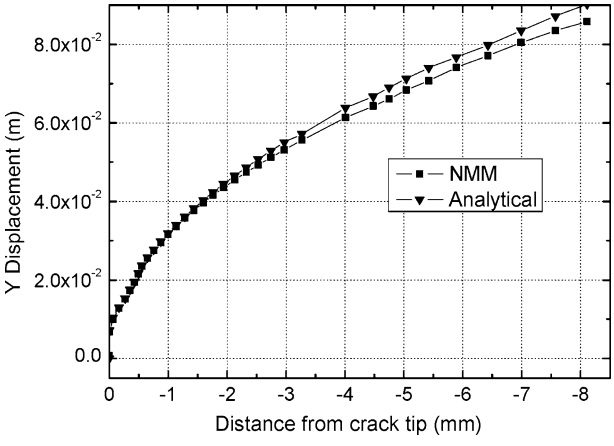

Fig. 13 Y-displacements behind the crack tip for the edge crack problem

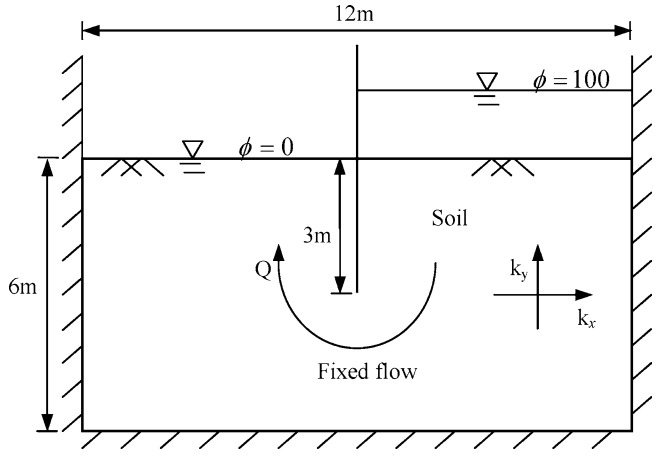

Fig. 14 The problem of the underground water

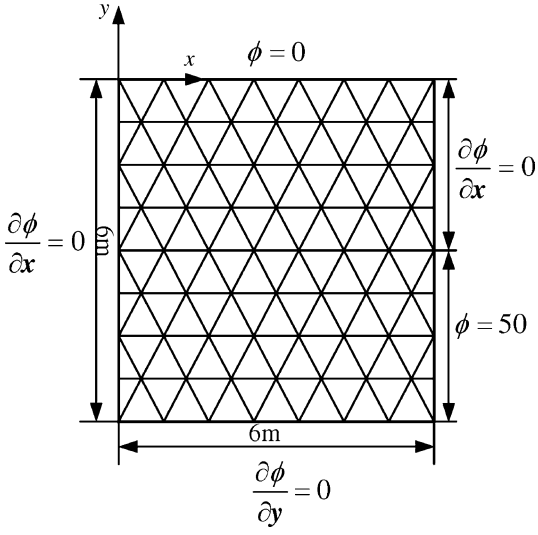

Fig. 15 Manifold elements and boundaries of the left half model

6.3 Groundwater modeling

An example from the literature (Smith, 1998) is used to show the effectiveness of the proposed method in modeling problems of ground water flow. The two-dimensional groundwater flow system is shown in Fig. 14. The total water head is 100 m, and permeability coefficient of the soil is 1 m/day.

The problem is governed by the equation

$$\frac{\partial^2 \phi}{\partial x^2} + \frac{\partial^2 \phi}{\partial y^2} = 0, \quad (x, y) \in [0, 12] \times [0, 6] \tag{71}$$

Due to symmetry, only half of the field on the left hand side is modeled. The NMM model is shown in Fig. 15, where 100 triangular meshes and 1st order displacement approximation are used in the model. The spring stiffness for both normal and shear directions is 1.0×10^7 N/m. The maximum allowed flow ratio in a step is 0.01 percent.and 3000 steps with time interval $\Delta t = 0.01$ s have been used in the calculation.

Table 2 The flux and the velocity of flow by different numerical methods

	Manifold method (m3/day)	Finite element method (m3/day)	Analytical solution (m3/day)
Inflow	−49.67	−48.57	
Outflow	49.67	48.57	
flow rate	49.7	48.6	50

The results from the numerical manifold method are compared with that from the finite element method (Smith, 1998) in Table 2. By comparing the manifold element solutions to the finite element solutions using linear triangular elements, it can be seen that the manifold element is more accurate than the finite element in the example. The reason is that the 1st order approximation functions of the triangular element in the NMM have the same precision as that of quadratic approximations of the triangular element in the FEM.

7 Conclusions

The derivation of the governing equations of the NMM from the weighted residual method leads to the same result as that derived from the minimum potential energy principle by choosing suitable weight functions. This is demonstrated in the paper for the linear elasticity problem.

For many applied problems, the governing equation of NMM cannot be derived from the minimum potential energy principle. One typical example is the case of Laplace's equations. The NMM formulation for Laplace's equation is developed in this paper by the method of weighted residual. Laplace's equation is a general equation governing various physical natures. These differential equations can represent heat conduction and potential flow, etc. Therefore, the manifold element formulation of the Laplace equation paves the way for the application of the NMM to a wider range of problems.

In the MWRs, the choice of weight function W_i is abundant and convenient. Using different weight function, different governing equations of NMM can be formed. The method developed in this paper enriches the mathematical foundation of the NMM and extends its field of applications.

References

Belytschko T, Lu YY, Gu L (1994) Element-free Galerkin methods. Int J Numer Meth Eng 37: 229–256

Yumin C, Aixiang H (1996) Boundary element analysis package BESMAP and its engineering application Journal of tongji university, 24(6): 726–730 (in Chinese)

Guanqi C, Ohnishi Y, Ito T (1998) Development of high-order manifold method. Int J Numer Meth Eng 43: 685–712

Yaw-Jeng C, Yu-Min L, Ren-Jow T (2002) Mixed mode fracture propagation by manifold method. Int J Fracture. 114: 327–347.

Ewalds H, Wanhill R (1989) Fracture Mechanics. Edward Arnold: New York

Cheng-yu K (2001) Modeling of jointed rock mass based on the numerical manifold method. Ph.D, University of Pittsburgh

Xing J, Yumin C (1997) The develop of boundary element method and its program£®Shanghai, Tongji University press (in Chinese)

Jeen-Shang L (2003) A mesh-based partition of unity method for discontinuity modeling. Comput Meth Appl Mech Eng 192: 1515–1532

Shi GH (1992) Modeling Rock Joints and Blocks by Manifold Method. Proceedings of 32nd U.S. Symposium on Rock Mechanics. Santa Fe, New Mexico 639–648

Shi GH (1996) Manifold method of material analysis. In: Proc. of IFDDA'1996. Berkeley, California, USA, pp. 52–204

Shi GH (1997) Numerical manifold method. Proc. of the second international conference on analysis of discontinuous deformation, Kyoto, Japan pp. 1–35

Shi GH (1998) Discontinuous deformation analysis: a new numerical model for the statics and dynamics of block systems. Ph.D., University of California, Berkeley

Smith IM, Griffiths DV (1998) Programming the finite element method. Third edition, John Wiley & Sons, Inc.

Kenjiro T, Asai M, Yamagishi M (2003) Finite cover method for linear and non-linear analyses of heterogeneous solids. Int J Numer Meth Eng 58: 1321–1346.

Xu ci-da 1987 WMR in solid mechanics. Shanghai, Tongji university press, (in Chinese)

Zienkiewicz OC (1977) The Finite Element Method in Engineering. London: 3nd (edn.) McGraw-Hill